S K-edge XAS as a Probe of Ligand-Metal Bond Covalency: Metal vs Ligand Oxidation in Cu and Ni Dithiolene Complexes

Ritimukta Sarangi[†], **Serena DeBeer George**[§,*], **Deanne Jackson Rudd**[†], **Robert K. Szilagyi**[†,‖], **Xavi Ribas**[⊥], **Concepció Rovira**[⊥,ζ], **Manuel Almeida**[ƒ], **Keith O. Hodgson**[†,§,*], **Britt Hedman**[§,*], and **Edward I. Solomon**[†,§,*]

[†]Department of Chemistry, Stanford University, Stanford, CA 94305

[§]Stanford Synchrotron Radiation Laboratory, Stanford Linear Accelerator Center, Stanford University, Stanford, CA 94309

[⊥]Institut de Ciència de Materials de Barcelona, Campus de la Universitat Autònoma de Barcelona, 08193 Bellaterra, Spain

[ƒ]Departamento de Química, Instituto Tecnológico e Nuclear, CFMC-UL, P-2686-953 Sacavém, Portugal

Abstract

A combination of Cu L-edge and S K-edge X-ray absorption data and density functional theory (DFT) calculations have been correlated with ^{33}S EPR superhyperfine results to obtain the dipole integral (I_s) for the S 1s→3p transition for the dithiolene ligand MNT (maleonitriledithiolate) in (TBA)$_2$[Cu(MNT)$_2$]. The results have been combined with the I_s of sulfide derived from XPS studies to experimentally obtain a relation between the S 1s→4p transition energy (which reflects the charge on the S atom (Q_{mol}^S)) and the dipole integral over a large range of Q_{mol}^S. The results show that for high charges on S, I_s can vary from the previously reported I_s calculated using data over a limited range of Q_{mol}^S. A combination of S K-edge and Cu K and L-edge X-ray absorption data and DFT calculations have been used to investigate the one-electron oxidation of [Cu(MNT)$_2$]$^{2-}$ and [Ni(MNT)$_2$]$^{2-}$. The conversion of [Cu(MNT)$_2$]$^{2-}$ to [Cu(MNT)$_2$]$^-$ results in a large change in the charge on the Cu atom in the molecule (Q_{mol}^{Cu}) and is consistent with a metal-based oxidation. This is accompanied by extensive charge donation from the ligands to compensate the high charge on the Cu in [Cu(MNT)$_2$]$^-$ based on the increased S K-edge and decreased Cu L-edge intensity, respectively. In contrast, the oxidation of [Ni(MNT)$_2$]$^{2-}$ to [Ni(MNT)$_2$]$^-$ results in a small change in Q_{mol}^{Ni} indicating a ligand-based oxidation consistent with oxidation of a molecular orbital, ψ_{SOMO}^* (singly occupied molecular orbital), with predominant ligand character.

[*]To whom correspondence should be addressed Fax: (650) 725-0259, Edward.solomon@stanford.edu; Fax: (612) 625-5780,.

[‖]Current address: Department of Chemistry and Biochemistry, Montana State University, Bozeman, MT 59717, USA

[ζ]Current address: Departament de Química, Campus Montilivi, Universitat de Girona, 17071 Girona, Spain

Supporting Information Available: Fits to the Cu K-edge shakedown and 1s→4p transitions for **1** and **1ox**. Comparison of S K-edge data of free (TBA)$_2$[MNT], **1** and **1ox**. Comparison of S K-edge data of **2**, **2ox** and [Ni(S$_2$C$_2$Me$_2$)]$^{-,2-}$. Pseudo-Voigt fits to all S K- and Cu L-edge data. Correlation plot of $Q_{free-ion}^S$ and S(1s) and S(4p) orbital energy gap. DFT optimized structures. Results obtained from B3LYP calculations. Comparison of S character in the $\psi_{\beta-LUMO}^*$ of [Ni(S$_2$C$_2$Me$_2$)]$^{0,-,2-}$ using the previously reported and spectroscopically determined I_s. Details of the S 1s→4p transition energy assignment in **1**. Full author list for reference [36]. This material is available free of charge via the Internet at http://pubs.acs.org.

1 Introduction

Ligand K-edge X-ray absorption spectra of transition metal complexes often display intense pre-edge features.[1,2] In the case of S K-edge X-ray absorption spectra, these features occur due to electric dipole allowed transitions from the S 1s to the formally filled S 3p orbital which mix into the metal d-orbitals due to bonding. Since the transitions under consideration are localized on the S atom, the pre-edge intensity reflects the amount of S character in these partially occupied or unoccupied metal d orbitals and thus the metal-S covalency.[3,4] This methodology has been applied to various systems with metal-S bonds and the S characters in the ground state wave functions have been successfully determined making S K-edge XAS a powerful spectroscopic technique.[5-7]

The ground state wave function ($\psi^*_{\beta-LUMO}$) (*i.e* the β-spin lowest unoccupied molecular orbital in a spin-unrestricted description) of a metal complex with a S containing ligand with one hole in the $3d$ orbital (for example, any d^9 Cu(II)-S(R) complex) can be written as:

$$\psi^*_{\beta-LUMO}=\left[1-\beta^2-\alpha^2\right]^{1/2}\phi\left(Metal\left(3d\right)\right)-\beta\phi\left(S\left(3p\right)\right)-\alpha\phi\left(Non-S\left(Ligands\right)\right)$$

Here β^2 corresponds to the amount of S character, α^2 the amount of the remaining part of the S containing ligand and [1-β^2- α^2] the amount of metal 3d character in the $\psi^*_{\beta-LUMO}$. The observed pre-edge transition intensity ($I\left[S\left(1s\rightarrow\psi^*_{\beta-LUMO}\right)\right]$) is then the intensity of the pure electric dipole-allowed S 1s→3p transition ($I[S(1s\rightarrow3p)]$) weighted by β^2.

$$I\left[S\left(1s\rightarrow\psi^*_{\beta-LUMO}\right)\right]=\beta^2 I\left[S\left(1s\rightarrow3p\right)\right]$$

The value of β^2 (percent S(3p) character) can be quantitatively determined from two parameters; the total integrated area under the S-K pre-edge peaks and the dipole integral (I_s) (gives the intensity of an electric dipole allowed transition) for the 1s→3p transition for the S species under consideration. The I_s has been quantitatively determined for sulfide (S^{2-}) using a valence bond configuration interaction analysis of 2p photoelectron spectra of KFeS$_2$.[8] Also, the dipole integral of thiolate (RS$^-$) in plastocyanin has been determined using S K-edge XAS data of a copper thiolate model complex, [Cu(tet$b$)(o-SC$_6$H$_4$CO$_2$)](H$_2$O).[9] Since I_s increases with an increase in the charge on sulfur, and increased charge on sulfur leads to an increase in the 1s→4p transition energy (see section 4.1 fordetails), a linear correlation between the I_s and S 1s→4p transition energies is expected. Using this relation and the above calibrations as references, the dipole integral term for S in different ligand environments has been determined. However, since both sulfide and thiolate have relatively high negative charges on S, this method needs to be experimentally extended to include S ligands which have high positive charge as part of the calibration of I_s. In this study, our S K-edge methodology is extended to include maleonitriledithiolate (MNT), a cyano substituted dithiolene ligand system. [Cu(MNT)$_2$]$^{2-}$ has been extensively studied by EPR and ENDOR methods and the S character in the ground state wavefunction has been determined from ^{33}S EPR superhyperfine data analysis.[10-14] These data are used to calibrate the pre-edge intensity obtained for [Cu(MNT)$_2$]$^{2-}$ and to determine the I_s for the dithiolene ligand.

Dithiolene ligand systems have been extensively studied over the last ~40 years due to their non-innocent bonding with transition metals.[15-20] In particular, the role of the dithiolene ligand in stabilizing the one- and two-electron oxidized forms of various $[Ni(dithiolene)_2]^{2-}$ systems has been under considerable debate.[21-24] In a recent study, we experimentally found that the ground states of $[Ni(S_2C_2Me_2)_2]^{0,1-,2-}$ reflect the strong covalent overlap between Ni and $(S_2C_2Me_2)^{2-}$. We also showed that there is a strong electrostatic repulsion between the two S atoms in individual $(S_2C_2Me_2)^{2-}$ ligands (which are situated close to each other due to a rigid C=C framework) which leads to inverted bonding with the Ni d-orbitals lower in energy than the dithiolene ψ^*_{HOMO} (highest occupied molecular orbital). These two factors lead to primarily ligand-based (mostly S) one- and two-electron oxidations of $[Ni(S_2C_2Me_2)_2]^{2-}$.[25] In the present study, the electronic structure change upon oxidation of $[Cu(MNT)_2]^{2-}$ to $[Cu(MNT)_2]^{-}$ is investigated using Cu K- and L-edges in addition to S K-edge X-ray absorption spectroscopy see Scheme 1. The data are combined with DFT calculations to gain insight into the role of the ligand in stabilizing the hole created upon oxidation. Additionally, the experimentally derived I_s for MNT is used to quantify the covalencies for $[Ni(MNT)_2]^{n-}$ systems and to re-evaluate the covalencies for the $[Ni(S_2C_2Me_2)_2]^{n-}$ systems. These studies show that while the formal oxidation states of $[Cu(MNT)_2]^-$ and $[Ni(MNT)_2]^-$ are Cu(III) and Ni(III), respectively, (shown in Scheme 1) the ligand plays a non-innocent role in bonding and the one-electron oxidation of $[Cu(MNT)_2]^{2-}$ and $[Ni(MNT)_2]^{2-}$ lead to metal and ligand-based oxidation, respectively. The factors contributing to this difference in redox behavior are discussed and the specific factors involed in a non-innocent ligand system which would lead to ligand-centered vs metal-based oxidation are considered.

2. Experimetal Section

2.1 Sample preparation

$(TBA)_2[Cu(MNT)_2]$ (**1**), $(TBA)[Cu(MNT)_2]$ (**1ox**) $(NEt_4)_2[Ni(MNT)_2]$ (**2**) and $(NEt_4)[Ni(MNT)_2]$ (**2ox**) [MNT= Maleonitriledithiolate, TBA= tetra n-butyl ammonium, Et= ethyl] were synthesized as previously described.[26,27] All complexes are stable at room temperature and were handled on the bench top during sample preparation. For Cu K-edge XAS measurements, the solid samples were finely ground with BN into a homogeneous mixture and pressed into a 1 mm Al spacer between 37 μm Kapton tape. The samples were frozen and stored under liquid N_2. During data collection, the samples were maintained at a constant temperature of 10 K using an Oxford Instruments CF 1208 liquid helium cryostat. The Cu L-edge samples were similarly handled and spread thinly over double-sided adhesive conducting graphite tape on an Al sample paddle. The paddles were affixed to a rotary stage and transferred into a vacuum chamber. The samples were positioned at 45° to the incident beam. The S K-edge samples were ground finely and dispersed as thinly as possible on Mylar tape to minimize the possibility of self absorption effects.

2.2 Cu K-edge

The Cu K-edge X-ray absorption spectra of **1** and **1ox** were measured at the Stanford Synchrotron Radiation Laboratory (SSRL) on the unfocussed 8-pole 1.8 T wiggler beam line 7-3 under ring conditions of 3 GeV and 60-80 mA. A Si(220) double crystal monochromator was used for energy selection. The monochromator was detuned 50% at 9987 eV to reject components of higher harmonics. Transmission mode was used to measure data to $k = 16$ Å^{-1}. Data represented here are a three-scan average spectrum. Achievement of internal calibration, background subtraction and data normalization were performed as described in earlier publications.[28] The data were normalized using the *SPLINE* program in the XFIT suite of programs.[29] Theoretical EXAFS signals $\chi(k)$ were calculated using *FEFF* (version 7.0)[30,31] and fit to the data using *EXAFSPAK*.[32] The distance obtained from the EXAFS analyses of

these data (not shown) were in excellent agreement with those obtained from crystal structure parameters and confirmed the sample integrity.

2.3 Cu L-edge

Cu L-edge X-ray absorption spectra of **1** and **2** were recorded at SSRL on the 31-pole wiggler beam line 10-1 under ring operating conditions of 50-100 mA and 3 GeV using a spherical grating monochromator with 1000 lines/mm and set at 30 μm entrance and exit slits. Sample measurements were performed using total electron yield where the sample signal (I_1) was measured with a Galileo 4716 channeltron electron multiplier aligned at 45° relative to the copper paddle. The mode of data collection and achievement of external calibration were performed as described in earlier publications.[33] Spectra presented here are 3-5 scan averages, which were processed using the *SPLINE* program in the XFIT suite of programs by fitting a second-order polynomial to the pre-edge region and subtracting it from the entire spectrum as background, resulting in a flat post-edge.[29] The data were normalized to an edge jump of 1.0 at 1000 eV. The normalized data were then processes in Microsoft Excel. Two arctangents were subtracted from the data which were separated by $3/2*\lambda_{L.S}$ (20.25 eV) and fixed with an $L_3:L_2$ intensity ratio of 2:1. The total integrated area was obtained between 930-950 eV. Normalization procedures introduce ~5% error in the value of the total integrated area.

2.3 S K-edge

S K-edge data of **1-2ox** were measured using the SSRL 54-pole wiggler beamline 6-2 in high magnetic field mode of 10 kG with a Ni-coated harmonic rejection mirror and a fully tuned Si (111) double crystal monochromator. Details of the optimization of this beam line for low energy fluorescence measurements and the experimental setup have been described previously. [34] External energy calibration and data normalization were performed as described in earlier publications.[5,35] The area under the pre-edge peak was quantified by fitting the data using *EDG_FIT*.[32] The pre-edge and rising edge features were modeled with pseudo-Voigt line-shapes with a fixed 1:1 Lorentzian:Gaussian ratio. The reported intensity and half-width values are based on an average over simultaneous fits that accurately modeled the data and their second derivative. Normalization procedures introduce ~3% error in the value of the integrated area under the pre-edge peak. The error is larger (~6%) in the case of **2ox** due to the overlap of pre-edge and edge transitions.

2.4 Electronic Structure Calculations

Gradient-corrected, (GGA) spin-unrestricted, broken symmetry, density functional calculations were carried out using the Gaussian03[36] package on a 2-cpu linux computer. Geometry optimizations were performed for each complex. The Becke88[37,38] exchange and Perdew86[39,40] correlation non-local functionals with Vosko-Wilk-Nusair[41] local functionals as implemented in the software package (BP86) were employed in this study to compare the electronic structure differences in **1**, **1ox**, **2**, and **2ox**. The triple-ζ 6-311G*[42-44] and the double-ζ 6-31G*[45-47] basis sets were used on the Cu, Ni and S atoms and the C, H and N atoms, respectively. Population analyses were performed by means of Weinhold's Natural Population Analysis (NPA)[48-50] including the Cu 4p orbitals in the valence set. Wave functions were visualized and orbital contour plots were generated in Molden.[51] Compositions of molecular orbitals and overlap populations between molecular fragments were calculated using the PyMOlize program.[52]

2.5 TD-DFT Calculations

TD-DFT calculations were performed with the electronic structure program ORCA.[53,54] Single point ground state DFT calculations with the BP86 functional were performed using the geometry optimized coordinates obtained from Gaussian03. The triple-ζ 6-311G* basis set was

used for all atoms. The symmetry equivalent S 1s orbitals were localized, and only excitations from the localized S 1s orbitals to the lowest unoccupied orbitals were allowed. Oscillator strengths for the individual S-K pre-edge transitions were obtained.

3. Results

3.1 [Cu(MNT)$_2$]$^{2-/-}$

3.1.1 Cu K-edge—A comparison of the normalized Cu K-edge X-ray absorption spectra of **1** (black) and **1ox** (red) is shown in Figure 1. The inset in Figure 1 shows the second derivative spectra of the pre-edge region. The pre-edge feature observed at ~8980 eV is a low-intensity (dipole-forbidden) quadrupole-allowed 1s→3d transition, which gains intensity from 4p mixing into the d-manifold due to deviation from centrosymmetry.[55] This pre-edge feature occurs at 8979.3 eV in **1** while it is shifted to higher energy by ~1.4 eV and appears at 8980.7 eV in **1ox**. The intense rising edge feature observed at ~8985 eV is a result of a formally two electron 1s→4p+ligand-to-metal charge transfer (LMCT) shakedown transition which becomes allowed due to final-state relaxation.[28,56] This feature appears at 8985.0 eV in **1** while it is shifted up in energy by 1.6 eV in **1ox** and occurs at 8986.6 eV. In addition to the shift in energy, the intensity ratio between the intense shakedown transition to the rising edge main transition increases on going from **1** to **1ox**, (Figure S1, Supporting Information).

3.1.2 Cu L-edge—Figure 2 shows a comparison of the normalized Cu L-edge X-ray absorption spectra of **1** (black) and **1ox** (red). The spectrum of the well characterized D_{4h} [CuCl$_4$]$^{2-}$ complex (blue) has been included as a reference.[57] The L-edge spectrum reflects the metal 2p→3d dipole allowed transition and consists of two sharp spin-orbit split peaks separated by ~20 eV with an intensity ratio of ~2:1. The L$_2$ edge (~950 eV) is broadened due to an additional Auger decay channel of the excited state which is absent for the L$_3$ edge (~930 eV).[58] The L$_3$ edge occurs at 931.7 eV in **1** and is shifted up by ~1.6 eV to 933.3 eV in **1ox**.

The L-edge intensity reflects the extent of metal-ligand covalent mixing. Due to the localized nature of the $2p \rightarrow \psi^*_{\beta-LUMO}$ transition, as the unoccupied metal 3d orbitals mix with filled ligand orbitals, the metal character decreases and the intensity of the L-edge transition decreases. A correlation of the total area under the L-edge of **1** and **1ox** with the total area of D_{4h} [CuCl$_4$]$^{2-}$ (well studied by various spectroscopic methods with $61 \pm 4\%$ Cu character in the $\psi^*_{\beta-LUMO}$) gives a quantitative estimate of the amount of Cu character in the ground state of **1** and **1ox**.[57,59,60] The total integrated area under the L-edges of **1** and **1ox** are 7.84 and 11.71 (Table 1), respectively which quantitate to a total Cu character of 39% in **1** and 56% in **1ox**. Since **1ox** is a two-hole system, (in contrast to D_{4h} [CuCl$_4$]$^{2-}$ and **1** which are one-hole systems) the per-hole Cu character is 28%. In both cases the Cu character is lower than that of D_{4h} [CuCl$_4$]$^{2-}$, indicating that both **1** and **1ox** have significant dithiolene character in their ground state wavefunctions.

3.1.3 S K-edge—The normalized S K-edge X-ray absorption spectra of **1** (black) and **1ox** (red) are shown in Figure 3. A comparison of these spectra with that of the free dithiolene ligand (Na)$_2$[S$_2$C$_4$N$_2$], is shown in Figure S2 (Supporting Information). The spectra of all three compounds consist of multiple transitions between 2469 eV and 2474 eV. However the lowest energy feature in **1** and **1ox** is absent in the free ligand and corresponds to a transition from the S 1s to the $\psi^*_{\beta-LUMO}$. This transition occurs at 2470.4 eV for **1**, while it is 0.3 eV lower in energy in **1ox** and occurs at 2470.1 eV. In contrast, the two edge transitions that occur at 2471.5 eV and 2472.8 eV for **1** are shifted to ~0.5 eV higher energy in **1ox** and occur at 2472.1 eV and 2473.2 eV.

Due to the localized nature of the S 1s orbital and the fact that an s→p transition is electric-dipole allowed, the $1s \to \psi^*_{\beta-LUMO}$ transition will gain intensity if the ground state wavefunction has a significant contribution from the S 3p orbital. Thus, the area under the pre-edge peak ($1s \to \psi^*_{\beta-LUMO}$ transition) provides a measure of the S(3p) β^2 character (see equation 1) in the $\psi^*_{\beta-LUMO}$. The total integrated areas under the S-K pre-edge peaks of **1** and **1ox** are 0.63 and 1.41, respectively (Table 2). Since **1ox** is a two-hole system, the renormalized per-hole pre-edge intensity is 0.70. The higher per-hole S character in the $\psi^*_{\beta-LUMO}$ of **1ox** (0.7) compared to **1** (0.63) is consistent with the lower per-hole Cu character in the $\psi^*_{\beta-LUMO}$ of **1ox** compared to **1** obtained from the Cu L-edge analyses (see section 3.1.2).

3.2 [Ni(MNT)$_2$]$^{2-/-}$

3.2.1 S K-edge—The normalized S K-edge X-ray absorption spectra of **2** (black) and **2ox** (red) are shown in Figure 4. In **2** the pre-edge transition overlays with the lowest-energy edge transition which results in a single broad feature. However, the two peaks are better resolved in the second derivative (see Figure S3, Supporting Information). The energy position of the pre-edge transition was determined to be 2471.2 eV. This corresponds to a transition from the S 1s to the $\psi^*_{\beta-LUMO}$, which is unoccupied in **2**. Upon oxidation, this peak shifts to lower energy and a second, lower energy peak is observed at ~2470 eV (Figure 4). This peak corresponds to a transition from the S 1s orbital to the ψ^*_{HOMO} of **2** which becomes half-occupied upon oxidation. The intensity of this transition reflects a large amount of S character in this now half occupied orbital (ψ^*_{SOMO}, singly occupied molecular orbital). These two pre-edge features are separated by ~0.8 eV and occur at 2470.2 eV and 2471.0 eV. Similar to the S K-edge shift observed on going from **1** to **1ox**, on going from **2** to **2ox**, the edge transitions shift to ~ 0.4 eV higher energy and occur at 2471.8 eV and 2472.8 eV for **2** and 2472.1 eV and 2473.3 eV for **2ox**. The total integrated area under the single peak in **2** is 0.99 and the two peaks in **2ox** is 1.93 (Table 2). Thus, the total integrated area increases by almost a factor of two on going from **2** to **2ox**.

3.3 Density Functional Theory (DFT) Calculations

3.3.1 Geometry Optimization—Spin-unrestricted density functional calculations were performed on **1**, **1ox**, **2** and **2ox** to correlate with the spectroscopic results and probe their electronic structure differences. The geometry-optimized structural parameters are in good agreement with the experimental data. The relevant bond distances are presented in Table 3. The calculated Cu-S bond distances for **1** and **1ox** are 2.32 Å and 2.22 Å compared to 2.27 Å and 2.17 Å, respectively, in the X-ray crystal structure.[13,61] The calculated Ni-S bond distances for **2** and **2ox** are 2.19 Å and 2.17 Å compared to 2.18 Å and 2.17 Å, from crystallography.[27] The Cu-S bond distances become ~0.1 Å shorter upon one-electron oxidation of [Cu(MNT)$_2$]$^{2-}$ while there is a much smaller change in the Ni-S distance upon one-electron oxidation of [Ni(MNT)$_2$]$^{2-}$ (~0.02 Å). The S-C, C-C and C-N distances are in reasonable agreement with the crystal structure data (see Supporting Information for geometry optimized coordinates) and undergo very small changes upon oxidation of both [Cu(MNT)$_2$]$^{2-}$ and [Ni(MNT)$_2$]$^{2-}$.

3.3.2 Energy Level Diagram—Figure 5 shows a schematic of the energy level diagram for **1**, **1ox**, **2** and **2ox**. The empty β-orbitals, which have been probed by S-K pre-edge spectroscopy, are shown in color while the filled orbitals are in gray. In all four complexes the $\psi^*_{\beta-LUMO}$ are qualitatively similar and exhibit an in-plane strong σ-bonding interaction between the metal $3d_{x^2-y^2}$ and the S $3p_\sigma$ orbitals. The ψ^*_{HOMO} (highest occupied molecular orbital) in **1**, **1ox** and **2** and the ψ^*_{SOMO} (singly occupied molecular orbital) in **2ox** are also qualitatively similar and

consist of an out-of-plane π-bonding interaction of the metal $3d_{xz}$ orbital and the S $3p_\pi$ orbital. To compare the relative energies of the $\psi^*_{\beta-LUMO}$'s, the energies of the N 1s orbitals were aligned. This was possible since the contribution of N atom to bonding is very similar in all the four complexes and hence undergoes similar energy shifts (see section 3.3.3). The $\psi^*_{\beta-LUMO}$ of **1ox** is 0.85 eV lower in energy compared to **1**. The $\psi^*_{\beta-LUMO}$ of **2ox** is 0.5 eV lower in energy compared to **2**. These shifts are in qualitative agreement with the shifts observed in the S $1s \rightarrow \psi^*_{\beta-LUMO}$ transition (see Table 2).[62] In addition, the DFT calculated energy difference between the $\psi^*_{\beta-LUMO}$ and the ψ^*_{SOMO} of **2ox** is ~0.9 eV, which is in good agreement with the energy splitting of the two S-K pre-edge features in **2ox** (0.8 eV) (Figure 4 and Table 2).

3.3.3 Ground State Wavefunction

3.3.3.1 [Cu(MNT)$_2$]$^{2-/-}$: DFT calculations using the BP86 functional give ground state descriptions of **1** and **1ox** that are in reasonable agreement with experimental ground state properties. Results obtained using the B3LYP[38] functional are similar with small quantitative differences in the ground state wave function compositions (Table S1, supporting information). Table 3 summarizes the compositions of selected spin-down molecular orbitals for **1** and **1ox** obtained from a Mulliken population analysis. The $\psi^*_{\beta-LUMO}$ of the S=1/2 ground state of **1** consists of 37.6% Cu $3d_{x^2-y^2}$ and 52.0% S $3p_\sigma$ character. The remaining 10.4% is distributed over the non-S atoms of the MNT ligand. The large amount of S character in the ground state is consistent with the in-plane strong σ type interaction between the Cu $3d_{x^2-y^2}$ and S $3p_\sigma$ orbitals. The one-electron oxidation of **1** to **1ox** leads to an S=0 ground state. The resultant $\psi^*_{\beta-LUMO}$ orbital is qualitatively similar to that in **1** and involves the same set of atomic orbitals. However, the $\psi^*_{\beta-LUMO}$ of **1ox** quantitatively differs from that of **1** in that it contains 24.7% Cu $3d_{x^2-y^2}$ and 64.8% S $3p_\sigma$ character. The remaining 10.5% is distributed over the remaining atoms of the MNT ligand. These results are in excellent agreement with the Cu characters in the ground state wavefunctions obtained from the L-edge spectra (39% in **1** and 28% in **1ox**). These results are also consistent with the increased per-hole S character in the ground state of **1ox** relative to **1** as observed by an increase in the S-K pre-edge intensity in **1ox** (see section 3.1.3).

3.3.3.2 [Ni(MNT)$_2$]$^{2-/-}$: The compositions of the key orbitals obtained from a Mulliken population analysis of spin unrestricted DFT calculations using the BP86 functional for **2** and **2ox** are summarized in Table 3. Results obtained using the B3LYP functional are summarized in Table S1 (Supporting Information). The ground state of **2** is S=0 and contains 42.9% Ni $3d_{x^2-y^2}$ and 43.8% S $3p_\sigma$ character. The remaining 13.3% is distributed over the remaining atoms of the MNT ligand. The one-electron oxidation of **2** creates a hole in the ψ^*_{HOMO} to generate **2ox** (hole in ψ^*_{SOMO}, Figure 5) which has an S=1/2 ground state. The $\psi^*_{\beta-LUMO}$ and the ψ^*_{SOMO} of **2ox** contain 39.5% Ni $3d_{x^2-y^2}$ and 46.2% S $3p_\sigma$ and 31.2% Ni $3d_{xz}$ and 50.5% S $3p_\pi$ character, respectively. The remaining 14.3% ($\psi^*_{\beta-LUMO}$) and 18.2% (ψ^*_{SOMO}) are distributed over the remaining atoms of the MNT ligand.

3.3.4 [Ni(MNT)]$_2^-$ vs [Ni(S$_2$C$_2$Me$_2$)$_2$]$^-$: DFT calculations on both **2** and **2ox** show very covalent $\psi^*_{\beta-LUMO}$'s with significant S 3p characters (44% in **2** and 51 % in **3**) which are reflected by the intense S-K pre-edge transitions. In an earlier publication DFT studies were performed on [Ni(S$_2$C$_2$Me$_2$)$_2$]$^{n-}$ (n=0,1)[25] which showed similar bond distances, ground state wavefunctions and intense S-K pre-edge transitions as in their MNT counterparts in the current study. Despite very similar electronic and geometric structures, the S K-edge spectra of [Ni(MNT)$_2$]$^{-,2-}$ and [Ni(S$_2$C$_2$Me$_2$)$_2$]$^{-,2-}$ are different in the energy range of 2469 eV and 2474 eV (Figure S4, Supporting Information). To understand these differences, a comparison of the key

unoccupied β-orbitals of **2ox** and $[Ni(S_2C_2Me_2)_2]^-$ is given in Figure 6. The calculated energy splitting between the $\psi^*_{\beta-LUMO}$ and ψ^*_{SOMO} in **2ox** and $[Ni(S_2C_2Me_2)_2]^-$ is 0.9 eV and 1.4 eV, respectively, which is in reasonable agreement with the experimental energy splitting of 0.8 eV (**2ox**) and 1.0 eV ($[Ni(S_2C_2Me_2)_2]^-$). Due to the electron donating nature of the methyl substituents, $[S_2C_2Me_2]^-$ is a better donor than MNT which contains electron withdrawing cyano substituents. Thus, the $\psi^*_{\beta-LUMO}$ in $[Ni(S_2C_2Me_2)_2]^-$ is destabilized compared to **2ox**, consistent with a larger splitting between $\psi^*_{\beta-LUMO}$ and ψ^*_{SOMO}. In $[Ni(S_2C_2Me_2)_2]^-$, the lowest lying unoccupied orbital with significant S3p character is LUMO+4 which is ~2.4 eV higher in energy than the $\psi^*_{\beta-LUMO}$. In contrast, in **2ox**, significant S3p character is observed in the LUMO+2 and LUMO+3 orbitals, which are ~0.8 eV higher in energy than the $\psi^*_{\beta-LUMO}$ orbital. This is consistent with the low lying edge transitions present in the S K-edge data of **2ox** (1.1 eV higher than the $\psi^*_{\beta-LUMO}$ orbital) which correspond to S 1s→LUMO+3 and 1s→LUMO+4 transitions. Alternatively, the lowest energy edge transition in $[Ni(S_2C_2Me_2)_2]^-$ is the 1s→LUMO+4 transition which is well separated from the pre-edge features at ~2.5 eV higher energy.

4. Analysis

4.1 Quantitation of Dipole Integral

Single crystal EPR and ESEEM studies and [33]S ESR superhyperfine analyses estimated the total S character in the $\psi^*_{\beta-LUMO}$ orbital of $[Cu(MNT)]^-$ to be 54%.[10,14,63] This is in good agreement with the 39% Cu character obtained from the Cu L-edge analysis (considering that the non-S MNT ligands contribute ~11% (see section 3.3.3.1)). These data are also in agreement with the DFT calculated Mulliken populations of the $\psi^*_{\beta-LUMO}$ (37.6% Cu(3d), 52.0% S(3p) and 10.4% remaining ligand). The S-K pre-edge intensity, weighted by the transition dipole integral (I_s) for the 1s→3p transition, is a measure of the S(3p) character (β^2) in the $\psi^*_{\beta-LUMO}$. The relation between I_s and β^2 is given by $D_0=(A/3n)\beta^2 I_s$, where D_0 is the total area under the pre-edge transition, A is the number of holes (metal 3d or ligand np) and n is the number of absorbing S atoms. Using this relation, the S-K pre-edge intensity, and the S character from [33]S EPR results, the resultant S (1s→3p) I_s of [Cu(MNT)] is determined to be 14.1. The value of I_s depends on the charge on the S in the molecule which modulates the S 1s and 3p radial functions. The S 3p radial function can also depend on the nature of metal-S overlap (σ vs π) (*vide infra*). In a previous publication, we used a combination of PES and S K-edge pre-edge data for $KFeS_2$ to determine the I_s for the S^{2-} ligand to be 5.4.[8] Using these two experimentally derived I_s's (for $[Cu(MNT)]^{2-}$ and $KFeS_2$), a reasonably accurate estimate of the I_s of any S based ligand can be made based on a linear correlation of the 1s→4p energy (2472.3 eV for sulfide and 2476.6 eV for $[Cu(MNT)]^{2-}$, see Figure S2 in Supporting Information) with I_s. It has been shown using DFT calculations that an increase in positive charge on the absorbing S atom leads to a linear increase in the value of I_s.[64] This is due to the fact that an increase in the charge on the S atom will lead to a larger contraction of the valence 3p orbitals. This leads to better overlap of the 1s and 3p radial functions and hence increase in I_s. Again, an increase in charge on the S atom shifts the core 1s orbital to deeper binding energy relative to the valence 4p orbitals and in the process increases the 1s(core)→4p(valence) energy gap. To obtain the relationship between the charge on the S atom and the 1s→4p transition energy, DFT calculations were used to evaluate the correlation between the binding energies of the S 1s and S 4p manifolds without complication from ligand environment and other molecular effects.

Using partial charges in a spherically symmetric field, $Q^S_{free-ion}$ was modulated over a large range, and the theoretical relationship of the S 1s and S 4p binding energies was obtained and is presented in Figure S5. The correlation of $Q^S_{free-ion}$ and the difference in binding energy of

S 1s and S 4p orbitals was found to be close to linear with only an ~3% contribution from a quadratic component. This indicates that a near linear relationship holds between I_s and the S 1s→4p transition energy.

In order to assign the S 1s→4p transition energy of $(Na)_2[Cu(MNT)_2]$, the S K-edge spectra of the free MNT ligand $\{(Na)_2MNT\}$ and $(Na)_2[Cu(MNT)_2]$ were used as references (shown in Figure S2) and correlated to DFT calculations. In the case of $[MNT]^{2-}$ and $[Cu(MNT)]^{2-}$ the assignment of 1s→S-C(π)* and 1s→S-C(σ)* is complicated by the presence of low lying transitions due to S character mixed into the cyano substituent (see section 3.3.4). Thus, a comparison of the S K-edge XAS data and DFT calculations of $(Na)_2(S_2C_2H_2)$ and $(NEt)_4[Ni(S_2C_2Me_2)]$ has been made since the spectra of these complexes are not complicated by other low-lying S-based transitions. A detailed analysis is presented in the Supporting Information. In case of the free dithiolene ligand $[(C_2H_2S_2)^{2-}]$, the 1s→S-Cπ* and the 1s→S-Cσ* are separated by only ~0.3 eV and occur under the peak observed at ~2472.8 eV, while the 4p transition occurs ~1.6 eV to higher energy at ~2474.2 eV. In the case of the Ni bound complexes, $[Ni(C_2S_2Me_2)]^{0,-,2-}$, the S-C bond becomes shorter relative to the free ligand, destabilizing the S-Cσ* orbital and raising the 1s→S-Cσ* transition energy. This is accompanied by an increase in Q_{mol}^S, leading to an increase in the 1s→4p transition energy. Thus, in $[Ni(S_2C_2Me_2)]^-$, the two peaks at ~2472.6 eV and ~2474.2 eV spilt into three peaks at 2473.5 eV, 2474.7 eV and 2475.9 eV corresponding to the 1s→S-Cπ*, 1s→S-Cσ* and 1s→4p transitions, respectively. A similar shortening in the S-C bond is observed in the $[Cu(MNT)_2]^{2-}$ complex relative to the free ligand and in analogy to $[Ni(S_2C_2Me_2)]^-$, the 1s→S-Cσ* and the 1s→4p transitions have been assigned to the transitions at 2474.4 eV and 2476.6 eV (see Supporting Information, Section S1).

Using the two experimentally derived I_s's for $[Cu(MNT)]^{2-}$ (1s→4p at 2472.4 eV) and $KFeS_2$ (1s→4p at 2476.6 eV) and the linear correlation of the 1s→4p energy transition determined above, a reasonably accurate estimate of the I_s of any S based ligand can be made. Using this method the I_s for the free $\{(Na)_2MNT\}$, $(Na)_2(C_2H_2S_2)$ and $Na(C_2H_5S)$ have been determined and plotted in Figure 7 which shows the experimentally derived I_s (as red squares) and interpolated I_s (black circles) based on the 1s→4p energy position of these S(ligand) systems. This is compared to our previous correlation (white circles), which was derived from the experimental data of $KFeS_2$ and a comparison of experimental and theoretical results for plastocyanin and a related thiolate-Cu^{II} model complex.[9] The spectroscopically derived correlation of I_s with 1s→4p is more accurate relative to previously used correlation since sulfide and $[Cu(MNT)]^-$ cover a large range of charge on S (in contrast to sulfide and thiolate used for the previous correlation) and the I_s value for both has been derived from *direct* spectroscopic techniques.

It should be noted that the more accurate I_s deviates from the previously reported I_s by only a small fraction for lower charges on S. The I_s for the thiolate ligand system (RS$^-$) changes from 8.05 to 8.47 (Figure 7). This changes the covalency of a metal-thiolate system (such as in the blue copper proteins) by only 2%. However, for high charges on S, I_s is seen to deviate significantly. The I_s's of dithiolene ligands (MNT^{2-} and $(S_2C_2Me_2)^{2-}$) are slightly higher than the previously reported I_s's. This in effect decreases the Ni-S covalencies for the $[Ni(S_2C_2Me_2)]^{2-,1-,0}$ complexes,[25] and agrees better with the theoretical results in that study (see Table S2, Supporting Information).

Using the I_s value from the spectroscopically derived plot in Figure 7, the S character in the ground state wavefunction of **1**, **1ox** and **2** become 54%, 60% and 42%, respectively (Table 4). These are in good agreement with the ground state wavefunctions obtained from Mulliken population analyses (52.0%, 64.8% and 41% in **1**, **1ox** and **2**, respectively). Since DFT calculations indicate that the contribution of C and N atoms to the ground state in **1** and **1ox** is

~10% (Table 3), the remaining contribution of ~36% (**1**) and 30% (**1ox**) has to be from Cu, which is in good agreement with Cu L-edge data (39% (per-hole) for **1** and 28% (per-hole) for **1ox**). The S characters in the lower (ψ^*_{SOMO}) and higher ($\psi^*_{\beta-LUMO}$) energy pre-edge features of **2ox** are 71% and 47%, respectively. While the S character in the $\psi^*_{\beta-LUMO}$ orbital is in good agreement with the calculated value of 46%, the experimental Ni-S covalency in the ψ^*_{SOMO} (70%) is ~20% higher than calculated (~50.5%). TD-DFT calculations indicate that the oscillator strength for the $1s \rightarrow \psi^*_{SOMO}$ (π orbital) is 17% lower than that for the $1s \rightarrow \psi^*_{\beta-LUMO}$ transition (σ orbital). This may reflect a greater radial distortion in the π-orbitals than in the σ-orbitals.[65] Using this ratio of oscillator strength between π- and σ-orbitals of the dithiolene, the experimentally obtained S character in the ψ^*_{SOMO} orbital of **2ox** becomes 58%, which is in more reasonable agreement with the calculated value of 50.5%. This is consistent with ENDOR results which indicate that the S character in the ground state of **2ox** is 52%.[66] It should be noted that although this difference in oscillator strength between π- and σ-orbitals can overestimate the covalency for ligands with high Q^S_{mol} (e.g dithiolene), its effect on ligands with low Q^S_{mol} (e.g sulfide and thiolate) is small.

4.2 Metal vs Ligand Centered Redox

The one-electron oxidation of **1** to **1ox** leads to a shift in the Cu K- and L- pre-edge transitions to higher energy by ~1.5 eV. It has been shown that these pre-edge shifts, which are transitions to the $\psi^*_{\beta-LUMO}$, are a measure of the ligand field (LF) felt by the absorbing Cu atom in the molecule.[67] It is interesting to note that the S-K pre-edge, which is also a transition into the $\psi^*_{\beta-LUMO}$, is shifted to *lower* energy in **1ox** relative to **1** (~0.3 eV). The S-K pre-edge energy position is affected by three factors: LF, and the charges on the S (Q^S_{mol}) and the Cu (Q^{Cu}_{mol}) atoms in the molecule. An increase in ligand field strength shifts the S pre-edge transition to higher energy by destabilizing the $\psi^*_{\beta-LUMO}$, an increase in Q^{Cu}_{mol} shifts the transition to lower energy by increasing the binding energy of the 3d-manifold, and an increase in Q^S_{mol} shifts the transition to higher energy (chemical shift induced by a change in charge).[5,68] Since Cu K- and L- pre-edge shifts reflect changes in LF and the S K-edge energy shifts (obtained from Figure 3) reflect changes in Q^S_{mol}, these shifts can be used to uncouple the contribution of Q^{Cu}_{mol} to the S-K pre-edge shifts. This difference in Q^{Cu}_{mol} reflects the difference in the 3d manifold energy between **1** and **1ox** due to the different charges on Cu in the two complexes. Using the above relation, the d-manifold of **1ox** is calculated to be 2.3 eV lower in energy relative to **1**.

This difference in the d-manifold energy indicates a large increase in the Q^{Cu}_{mol} in **1ox** which is indicative of a metal centered oxidation. An oxidation of Cu[II] to Cu[III] is consistent with the ~ 0.1 Å shorter Cu-S distance in **1ox** compared to **1**. This decrease in bond distance increases the ligand field and destabilizes the d-manifold, which is manifested in the Cu K- and L- pre-edge shifts to higher energy (~1.5 eV). The total Cu character obtained from Cu L-edge intensities is higher in **1ox** (56%) compared to **1** (39%). This is also consistent with a metal-based oxidation since an increase is metal character is reflected by an increase in the total L-edge intensity. However, the per-hole Cu character is smaller in **1ox** (28%) compared to **1** (39%). The oxidation of **1** (Cu[II]) to **1ox** (Cu[III]) leads to extensive charge donation from the dithiolene ligands to compensate the increased positive charge on the Cu atom.

The one-electron oxidation of **2** to **2ox** leads to a shift in the S-K pre-edge $1s \rightarrow \psi^*_{\beta-LUMO}$ transition to higher energy by ~0.2 eV. Further, S K-edge XAS and DFT calculations show that the one-electron oxidation of **2** to **2ox** is very similar to that of $[Ni(S_2C_2Me_2)_2]^{2-}$ to $[Ni(S_2C_2Me_2)_2]^-$ (*vide supra*). This indicates that the difference in LF between $[Ni(S_2C_2Me_2)_2]^{2-}$ and $[Ni(S_2C_2Me_2)_2]^-$ can be used as a handle on the difference in LF between

2 and **2ox**. Ni K-edge XAS on $[Ni(S_2C_2Me_2)_2]^{2-}$ and $[Ni(S_2C_2Me_2)_2]^-$ show that the LF increases by ~0.3 eV upon oxidation of $[Ni(S_2C_2Me_2)_2]^{2-}$ (measured by the shift in the Ni-K pre-edge positions).[25] Combining this as a measure of the difference in LF between **2** and **2ox** with S K-edge energies of **2** and **2ox** as a measure of the change in Q_{mol}^S (Figure 4), the d-manifold of **2ox** is calculated to be 0.8 eV lower than in **2**, due to the change in Q_{mol}^{Ni}. This difference is much smaller than the 2.3 eV shift observed on going from **1** to **1ox** obtained above. This indicates that the perturbation in Q_{mol}^{Ni} is much smaller than in Q_{mol}^{Cu} upon oxidation. This is consistent with a smaller change in the Ni-S bond distance on going from $[Ni(MNT)_2]^{2-}$ to $[Ni(MNT)_2]^-$ (~0.02 Å compared to the ~ 0.1 Å decrease in the Cu-S distance on going from **1** to **1ox**). Thus, a combination of Cu K-, Ni K- and S K-edge energy shifts indicate that in contrast to **1**, the oxidation of **2** is predominantly ligand-based.

S-K pre-edge intensities of **1** and **1ox** give a direct comparison of the differences in the Cu-S covalency in the two complexes. The per-hole S character in the $\psi^*_{\beta-LUMO}$ of **1** (1-hole) and **1ox** (2-holes) is 54% and 60%, respectively. This is in reasonable agreement with DFT calculations which indicate that the S character increases from 52.4% in **1** to 64.8% in **1ox**. This increase in the total S character (66%) in the $\psi^*_{\beta-LUMO}$ is consistent with the decrease in the per-hole Cu character obtained from Cu L-edge analysis (see section 3.1.2). The per-hole S character in the $\psi^*_{\beta-LUMO}$ of **2** (2-holes) and **2ox** (2-holes) is 42% and 47%, respectively. This is in reasonable agreement with Mulliken population analyses which indicate that the S character increases from 43.8% in **2** to 46.2% to **2ox**. From S-K pre-edge intensities, the increase in the total S character in the $\psi^*_{\beta-LUMO}$ is ~10% on going from **2** to **2ox**. Upon oxidation of **2** to **2ox** a hole is created in the ψ^*_{SOMO}, which contains 58% S character (this incorporates the difference in the oscillator strength between π- and σ-orbitals, see section 4.1). These results are consistent with Mulliken population analyses which indicate that the ψ^*_{SOMO} consists of 50.5% S character and 18.2% C and N character (remaining atoms of the dithiolene ligand). These results are also consistent with ^{15}N and ^{13}C ENDOR results which indicate that the total C and N contribution is ~15% in the ground state of **2ox**. ENDOR studies also indicate that the Ni character in the ground state (ψ^*_{SOMO}) is 32% which is consistent with the 31.2% obtained from DFT calculated Mulliken population analyses.[66]

In our earlier publication, DFT calculations were performed on the bonding within the free dithiolene ligands $[S_2C_2(Me)_2]^{2-}$ and $[\{S_2C_2(Me_2)\}_2]^{4-}$ and their interaction with the metal in $[Ni(S_2C_2Me_2)_2]^{0,-,2-}$. These studies showed that the ψ^*_{HOMO} of $[\{S_2C_2(Me_2)\}_2]^{4-}$ is destabilized to higher energy due to strong repulsion between the two negatively charged S atoms in the $(S_2C_2Me_2)^{2-}$ ligand.[25] This results in an inverted bonding scheme in $[Ni(S_2C_2Me_2)_2]^{n-}$ complexes with the initially occupied ligand orbital at higher energy relative to the metal 3d orbitals. Since the geometric and electronic structures of $[Ni(S_2C_2Me_2)_2]^{-,2-}$ and $[Ni(MNT)_2]^{-,2-}$ are very similar the relative orbital energies of the metal and ligand orbitals in both these set of complexes are consistent with a ligand-based oxidation. This is also supported by the Ni K-rising edge energies, which are very similar for **2** and **2ox** indicating similar Q_{mol}^{Ni} in these complexes. In contrast, the one-electron oxidation of **1** to **1ox** is shown to be metal-based from Cu K-edge energy shifts. This process creates a hole in the $\psi^*_{\beta-LUMO}$ which contains an in-plane strong σ-type interaction between the Cu $3d_{x^2-y^2}$ and S $3p_\sigma$ orbitals. This strong interaction facilitates extensive charge donation from the dithiolene ligand into the Cu center to neutralize the increased charge on the metal due to oxidation. This is consistent with the increase in the per-hole S-K pre-edge and decrease in the Cu L pre-edge intensity. In contrast, the one electron oxidation of **2** to **2ox** creates a hole in the ψ^*_{SOMO} orbital of **2ox** which contains an out-of-plane weaker (relative to the σ-type interaction between the Cu $3d_{x^2-y^2}$ and

S $3p_\sigma$ orbital) π-type interaction between the Ni $3d_{xz}$ and S $3p_\pi$ orbitals. This weak interaction leads to predominant ligand character in the ψ^*_{SOMO} leaving the metal relatively unperturbed, which is consistent with the small change in the Q^{Ni}_{mol} between **2** and **2ox** and a dominantly ligand-based oxidation of **2**.[25]

5. Discussion

S K-edge XAS provides an experimental measure of S 3p character in unoccupied metal d orbitals in complexes with metal-S bonds. A quantitative measure of the S character is possible when both the area under the pre-edge peak(s) and accurate I_s values are known. Correlation of S K-edge XAS data with ^{33}S EPR superhyperfine and Cu L-edge results on **1** has enabled the quantitative estimate of the I_s for the dithiolene ligand, MNT in $[Cu(MNT)_2]^{2-}$. Using the correlation of Q^S_{mol} to the S 1s→4p edge energy position and the linear dependence of I_s on Q^S_{mol}, I_s values can now be experimentally established from the interpolation plot shown in Figure 7 (red). This figure also includes our previous correlation (black) which used a limited range of Q^S_{mol}. The different slopes of the two I_s versus 1s→4p edge energy plots emphasize the importance of experimentally determining accurate I_s values, especially in the case of ligands with high positive charge on the S atom. Thus, this study allows a quantitative extension of our S K-edge XAS methodology to a broader range of S-containing ligand systems.

A combination of Cu K- and L-edge and S K-edge XAS has been used to establish that a metal-based oxidation occurs upon one electron oxidation of **1** to **1ox**. The pre-edge and edge energy shifts observed in these XAS spectra have been used to experimentally uncouple the effect of a change in Q^{Cu}_{mol} from the effects of change in ligand field and Q^S_{mol}. It is found that the d-manifold of **1ox** is shifted to lower energy by ~2.3 eV relative to that in **1** indicating significant change in Q^{Cu}_{mol} upon oxidation. In an earlier publication we have shown that the core and valence orbital shifts due to change in Q^{Cu}_{mol} are very similar.[67] Thus, energy trends in Cu 2p XPS data can be used to investigate trends in 3d manifold energies. XPS data on Cu^{II} inorganic complexes and their Cu^{III} analogues are available, which show an ~ 1.5-2.0 eV shift upon one-electron oxidation.[69-72] Thus, the large shift of 2.3 eV clearly demonstrates that the conversion of **1** to **1ox** involves a dominantly metal-based oxidation. S K-edge XAS studies have been used in combination with previously published Ni K-edge data (Supporting Information of Reference 25) to determine that a predominantly ligand-based oxidation occurs upon conversion of **2** to **2ox**. These data show that the shift in Ni 3d-manifold upon oxidation of **2** to **2ox** is ~0.8 eV which is much smaller than the shift in the Cu 3d-manifold upon oxidation of **1** to **1ox** reflecting a smaller change in Q^{Ni}_{mol}. Mulliken population analysis and orbital contour plots obtained from spin-unrestricted DFT calculations show that the one electron oxidation of **1** and **2** lead to very different ground states. In **1ox** the ground state wavefunction is $\psi^*_{\beta-LUMO}$, which contains an in-plane strong σ anti-bond between the Cu $3d_{x^2-y^2}$ and S $3p_\sigma$ orbitals while in **2ox** the ground state wavefunction is ψ^*_{SOMO}, which contains an out-of-plane weaker π interaction between the Ni $3d_{xz}$ and S $3p_\pi$ orbitals. These differences in the redox active molecular orbitals strongly affect the redox properties of **1** and **2** and lead to a metal-based oxidation in the case of the $[Cu(MNT)]^-$ and a ligand-based oxidation in the case of $[Ni(MNT)]^-$.

Supplementary Material

Refer to Web version on PubMed Central for supplementary material.

Acknowledgments

References

1. Shadle SE, Hedman B, Hodgson KO, Solomon EI. J. Am. Chem. Soc 1995;117:2259–2272.

2. Glaser T, Hedman B, Hodgson KO, Solomon EI. Acc. Chem. Res 2000;33:859–868. [PubMed: 11123885]

3. Williams KR, Hedman B, Hodgson KO, Solomon EI. Inorg. Chim. Acta 1997;263:315–321.

4. Hedman B, Hodgson KO, Solomon EI. J. Am. Chem. Soc 1990;112:1643–1645.

5. DeBeer George S, Metz M, Szilagyi RK, Wang HX, Cramer SP, Lu Y, Tolman WB, Hedman B, Hodgson KO, Solomon EI. J. Am. Chem. Soc 2001;123:5757–5767. [PubMed: 11403610]

6. Solomon EI, Hedman B, Hodgson KO, Dey A, Szilagyi RK. Coord. Chem. Rev 2005;249:97–129.

7. Solomon EI, Szilagyi RK, DeBeer George S, Basumallick L. Chem. Rev 2004;104:419–458. [PubMed: 14871131]

8. Rose K, Shadle SE, Glaser T, de Vries S, Cherepanov A, Canters GW, Hedman B, Hodgson KO, Solomon EI. J. Am. Chem. Soc 1999;121:2353–2363.

9. Shadle SE, Penner-Hahn JE, Schugar HJ, Hedman B, Hodgson KO, Solomon EI. J. Am. Chem. Soc 1993;115:767–776.

10. Kirmse R, Stach J, Dietzsch W, Hoyer E. Inorg. Chim. Acta 1978;26:L53–L55.

11. Stach J, Kirmse R, Dietzsch W, Olk RM, Hoyer E. Inorg. Chem 1984;23:4779–4780.

12. Snaathorst D, Doesburg HM, Perenboom JAAJ, Keijzers CP. Inorg. Chem 1981;20:2526–2532.

13. Plumlee KW, Hoffman BM, Ibers JA, Soos ZG. J. Chem. Phys 1975;63:1926–1942.

14. Maki AH, Davison A, Edelstein N, Holm RH. J. Am. Chem. Soc 1964;86:4580–4587.

15. McCleverty JA. Prog. Inorg. Chem 1968;10:49–221.

16. Eisenberg R. Prog. Inorg. Chem 1970;12:295–369.

17. Olk RM, Olk B, Dietzsch W, Kirmse R, Hoyer E. Coord. Chem. Rev 1992;117:99–131.

18. Robertson N, Cronin L. Coord. Chem. Rev 2002;227:93–127.

19. White LK, Belford RL. J. Am. Chem. Soc 1976;98:4428–4438.

20. Schrauzer GN, Mayweg VP. J. Am. Chem. Soc 1965;87:1483–1489.

21. Balch AL, Holm RH. J. Am. Chem. Soc 1966;88:5201–5209.

22. Shupack SI, Williams R, Gray HB, Billig E, Clark RJH. J. Am. Chem. Soc 1964;86:4594–4602.

23. Stiefel EI, Waters JH, Billig E, Gray HB. J. Am. Chem. Soc 1965;87:3016–3017.

24. Herebian D, Wieghardt KE, Neese F. J. Am. Chem. Soc 2003;125:10997–11005. [PubMed: 12952481]

25. Szilagyi RK, Lim BS, Glaser T, Holm RH, Hedman B, Hodgson KO, Solomon EI. J. Am. Chem. Soc 2003;125:9158–9169. [PubMed: 15369373]

26. Davison A, Holm RH, Edelstein N, Maki AH. Inorg. Chem 1963;2:1227–&.

27. Billig E, Waters JH, Gray HB, Bernal I, Williams R. Inorg. Chem 1964;3:663–&.

28. DuBois JL, Mukherjee P, Stack TDP, Hedman B, Solomon EI, Hodgson KO. J. Am. Chem. Soc 2000;122:5775–5787.

29. Ellis PJ, Freeman HC. J. Synchrotron Rad 1995;2:190–195.

30. Mustre de Leon J, Rehr JJ, Zabinsky SI, Albers RC. Phys. Rev. B 1991;44:4146–4156.

31. Rehr JJ, Mustre de Leon J, Zabinsky SI, Albers RC. J. Am. Chem. Soc 1991;113:5135–5140.

32. George, GN. EXAFSPAK & EDG_FIT. Stanford Synchrotron Radiation Laboratory, Stanford Linear Accelerator Center, Stanford University; Stanford, CA 94309: 2000.

33. Wasinger EC, de Groot FMF, Hedman B, Hodgson KO, Solomon EI. J. Am. Chem. Soc 2003;125:12894–12906. [PubMed: 14558838]

34. Hedman B, Frank P, Gheller SF, Roe AL, Newton WE, Hodgson KO. J. Am. Chem. Soc 1988;110:3798–3805.

35. Gorelsky SI, Basumallick L, Vura-Weis J, Sarangi R, Hodgson KO, Hedman B, Fujisawa K, Solomon EI. Inorg. Chem 2005;44:4947–4960. [PubMed: 15998022]

36. Pople, JA., et al. Gaussian 03, revision C.02. 2004.

37. Becke AD. Phys. Rev. A 1988;38:3098–3100. [PubMed: 9900728]

38. Becke AD. J. Chem. Phys 1993;98:5648–5652.

39. Perdew JP, Burke K, Wang Y. Phys. Rev. B 1998;57:14999.

40. Perdew JP. Phys. Rev. B 1986;33:8822–8824.

41. Vosko SH, Wilk L, Nusair M. Can. J. Phys 1980;58:1200–1211.

42. Curtiss LA, McGrath MP, Blaudeau JP, Davis NE, Binning RC, Radom L. J. Chem. Phys 1995;103:6104–6113.

43. Krishnan R, Binkley JS, Seeger R, Pople JA. J. Chem. Phys 1980;72:650–654.

44. McGrath MP, Radom L. J. Chem. Phys 1991;94:511–516.

45. Hariharan PC, Pople JA. Theoret. Chimica Acta 1973;28:213–222.

46. Francl MM, Hehre WJ, Binkley JS, Gordon MS, DeFrees DJ, Pople JA. J. Chem. Phys 1982;77:3645–3665.

47. Rassolov VA, Pople JA, Ratner MA, Windus TL. J. Chem. Phys 1998;109:1223–1229.

48. Carpenter JE, Weinhold F. THEOCHEM 1988;169:41–62.

49. Foster JP, Weinhold F. J. Am. Chem. Soc 1980;102:7211–7218.

50. Reed AE, Curtiss LA, Weinhold F. Chem. Rev 1988;88:899–926.

51. Schaftenaar G, Noordik JH. Comput-Aided Mol. Des 2000;14:123–134.

52. Tenderholt, A. PyMOlyze. Stanford University; Stanford, CA-94305: 2005.

53. Neese, F. ORCA- An Ab-initio, DFT and Semiempirical Electronic Structure Package, Max-Planck Institut für Bioanorganische Chemie. Mülheim; Germany: Nov. 2004 Version 2.4, Revision 16, 2004

54. Neese F, Olbrich G. Chem. Phys. Lett 2002;362:170–178.

55. Shulman RG, Yafet Y, Eisenberger P, Blumberg WE. Proc. Natl. Acad. Sci. U.S.A 1976;73:1384–1388. [PubMed: 5720]

56. DuBois JL, Mukherjee P, Collier AM, Mayer JM, Solomon EI, Hedman B, Stack TDP, Hodgson KO. J. Am. Chem. Soc 1997;119:8578–8579.

57. George SJ, Lowery MD, Solomon EI, Cramer SP. J. Am. Chem. Soc 1993;115:2968–2969.

58. Coster D, Kronig RDL. Physica 1935;2:13–24.

59. Solomon EI. Comments Inorg. Chem 1984;3:227–320.

60. Shadle SE, Hedman B, Hodgson KO, Solomon EI. Inorg. Chem 1994;33:4235–4244.

61. Forrester JD, Zalkin A, Templeton DH. Inorg. Chem 1964;3:1507–1515.

62. The $\psi^*_{\beta\text{-}LUMO}$ of **2** is 1.0 eV higher in energy compared to **1**. The $\psi^*_{\beta\text{-}LUMO}$ of **2ox** is 1.2 eV higher in energy compared to **1ox**. These results are also in good agreement with the experimental shifts observed in the S K- pre-edge transition energies.

63. Reijerse EJ, Thiers AH, Kanters R, Gribnau MCM, Keijzers CP. Inorg. Chem 1987;26:2764–2769.

64. Neese F, Hedman B, Hodgson KO, Solomon EI. Inorg. Chem 1999;38:4854–4860. [PubMed: 11671216]

65. Ray, K.; DeBeer George, S.; Solomon, EI.; Wieghardt, K.; Neese, F. Manuscript Submitted

66. Huyett JE, Choudhury SB, Eichhorn DM, Bryngelson PA, Maroney MJ, Hoffman BM. Inorg. Chem 1998;37:1361–1367. [PubMed: 11670347]

67. Sarangi R, Aboelella N, Fujisawa K, Tolman WB, Hedman B, Hodgson KO, Solomon EI. J. Am. Chem. Soc 2006;128:8286–8296. [PubMed: 16787093]

68. Randall DW, DeBeer George S, Holland PL, Hedman B, Hodgson KO, Tolman WB, Solomon EI. J. Am. Chem. Soc 2000;122:11632–11648.

69. Christ, BV. Handbook of Monochromatic XPS Spectra. John Wiley & Sons; 2000.

70. Bianconi A, Castellano AC, Desantis M, Delogu P, Gargano A, Giorgi R. Solid State Commun 1987;63:1135–1139.

71. Sacher E, Klemberg-Sapieha JE, Cambron A, Okoniewski A, Yelon A. J. Electron Spectrosc. Relat. Phenom 1989;48:C7–C12.

72. Mizokawa T, Namatame H, Fujimori A, Akeyama K, Kondoh H, Kuroda H, Kosugi N. Phys. Rev. Lett 1991;67:1638–1641. [PubMed: 10044206]
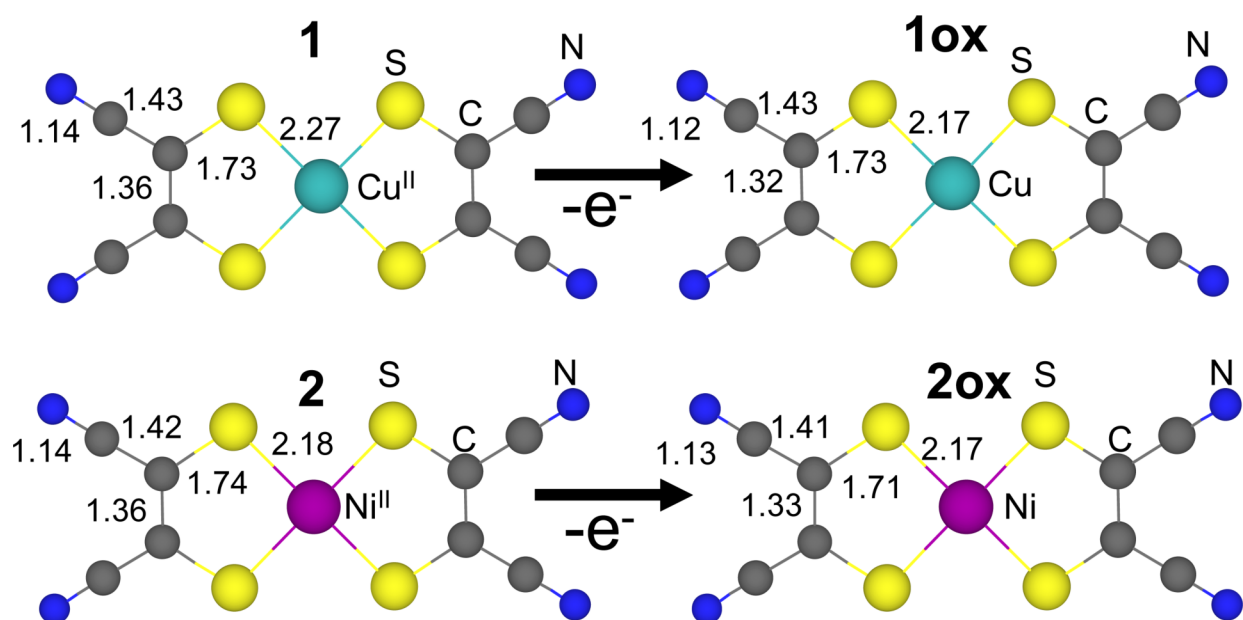
Scheme 1.
Ball and stick representation of $[Cu(MNT)_2]^{2-}$ (**1**), $[Cu(MNT)_2]^{-}$ (**1ox**), $[Ni(MNT)_2]^{2-}$ (**2**) and $[Ni(MNT)_2]^{-}$ (**2ox**). The formal oxidation state on the metal in **1ox** and **2ox** is Cu(III) and Ni (III), respectively.
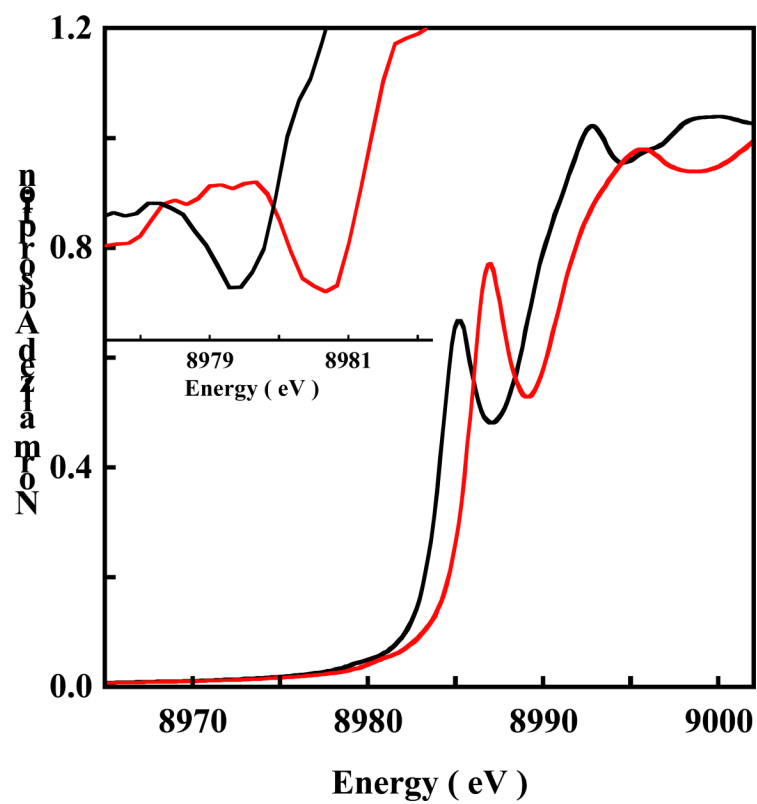
Figure 1.
The normalized Cu K-edge XAS spectra of (TBA)$_2$[Cu(MNT)$_2$] **1** (━━━━━) and (TBA)[Cu(MNT)$_2$] **1ox** (━━━━━). Inset shows the second derivative of the pre-edge region (1s → 3d transition, ~8978-8982 eV) indicating a ~1.4 eV shift.
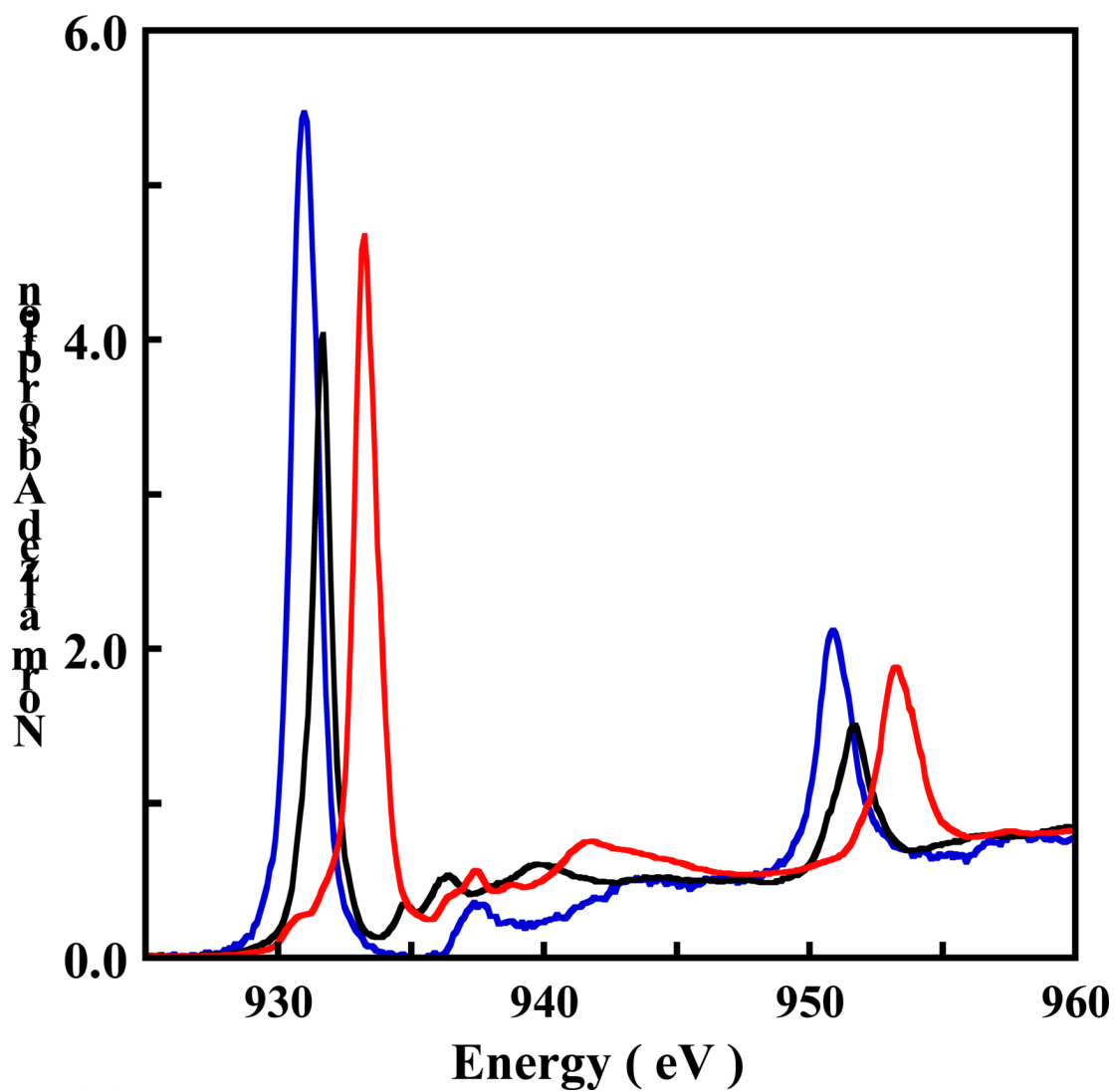
Figure 2.
The normalized Cu L-edge XAS spectra of $(TBA)_2[Cu(MNT)_2]$ **1** (⬛⬛⬛⬛) and (TBA)
$[Cu(MNT)_2]$ **1ox** (🟥🟥🟥) and D_{4h} $[CuCl_4]^{2-}$ (🟦🟦🟦). The intense peaks at
~ 930 eV and ~ 950 eV represent the L_3 edge ($2p_{3/2} \rightarrow$ 3d transition) and L_2 edge ($2p_{1/2} \rightarrow$ 3d
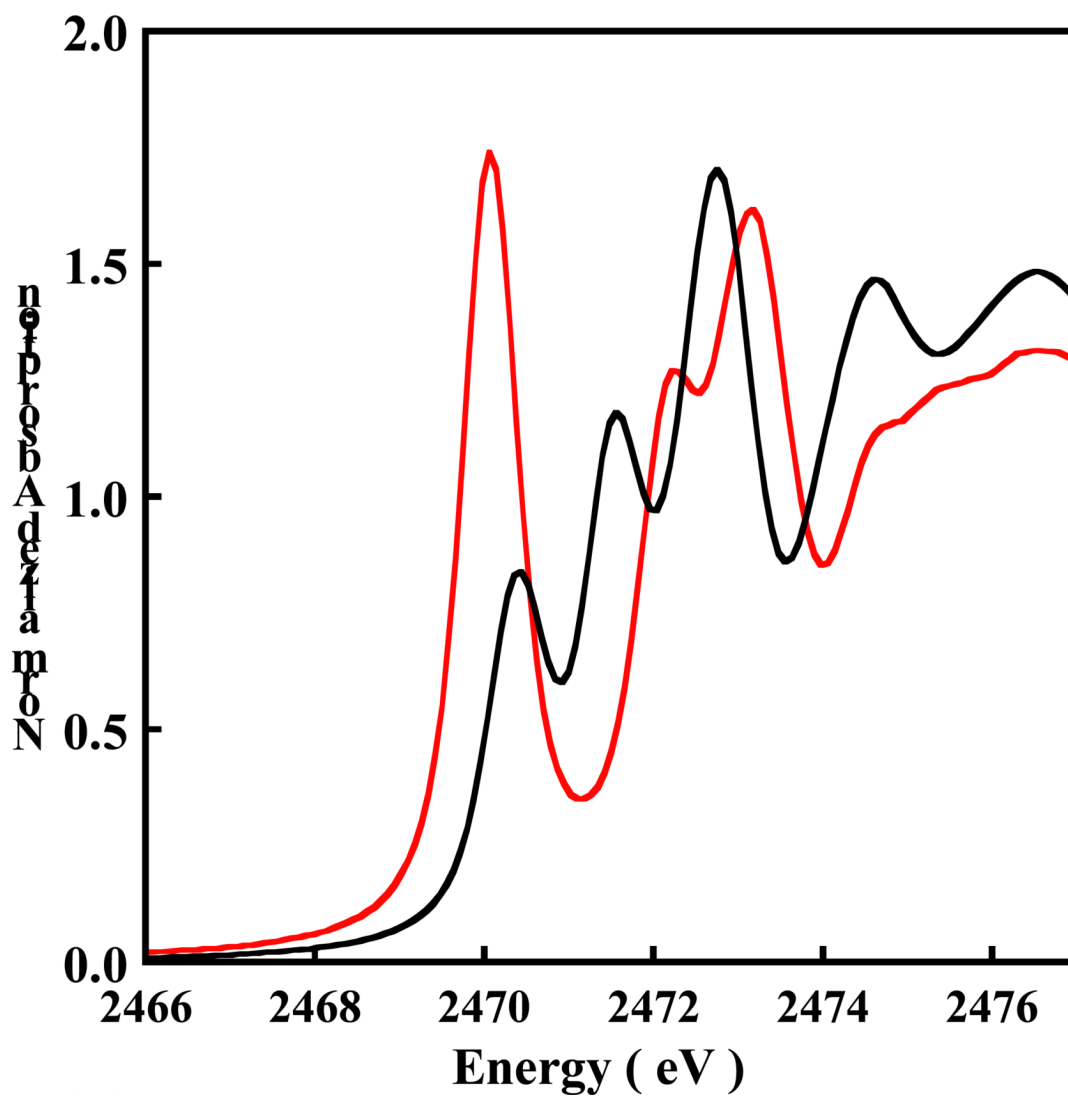transition), respectively.

Figure 3.
The normalized S K-edge XAS spectra of $(TBA)_2[Cu(MNT)_2]$ **1** (━━━━━) and (TBA)
$[Cu(MNT)_2]$ **1ox** (━━━━━). The intense peaks between 2471-2474 eV represent the
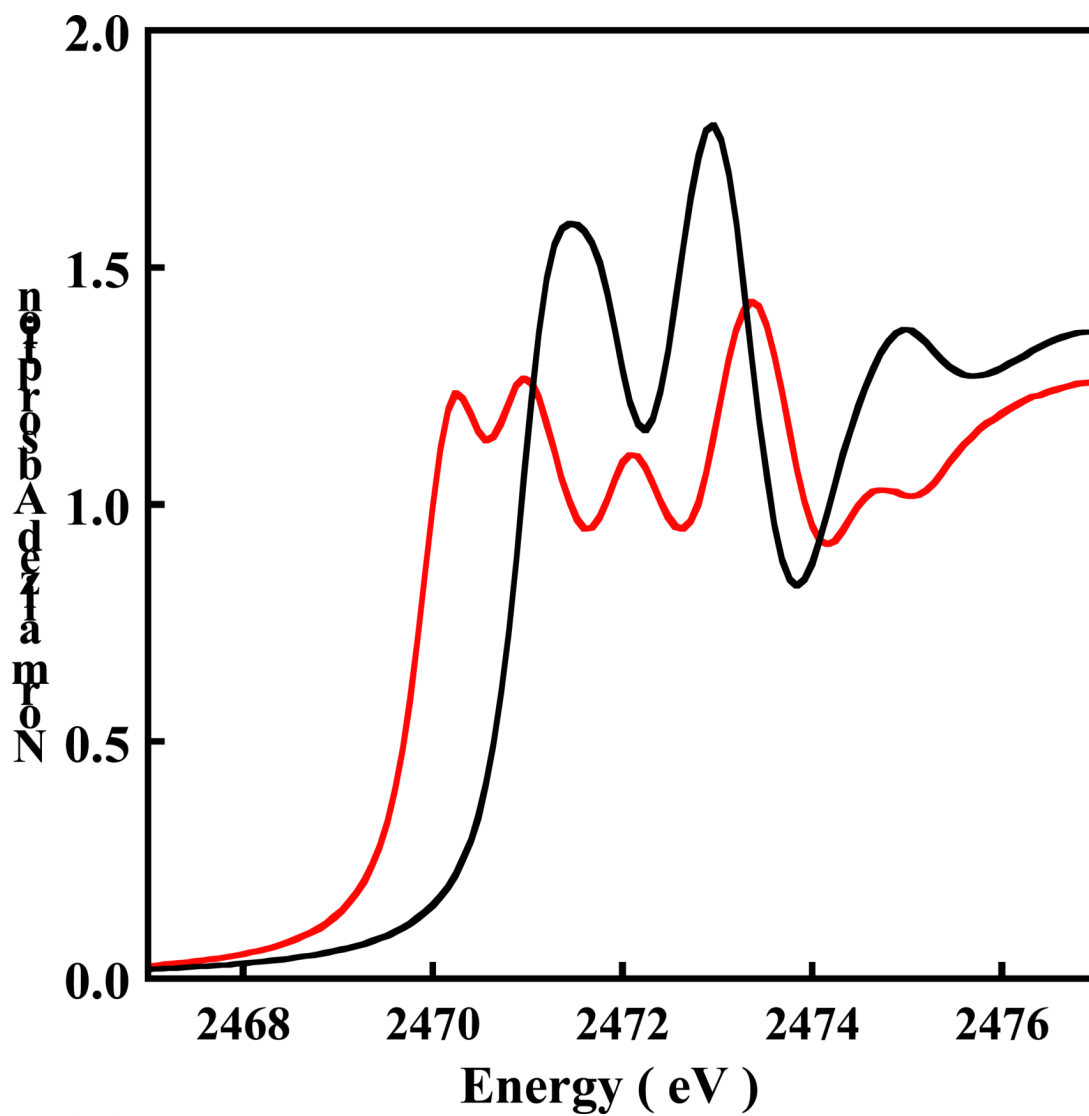low lying edge transitions (section 3.2).

Figure 4.
The normalized S K-edge XAS spectra of $(NEt_4)_2[Ni(MNT)_2]$ **2** (⬛️) and (NEt_4) $[Ni(MNT)_2]$ **2ox** (🟥). The pre-edge feature in **2** is buried in the lowest-energy edge transition.
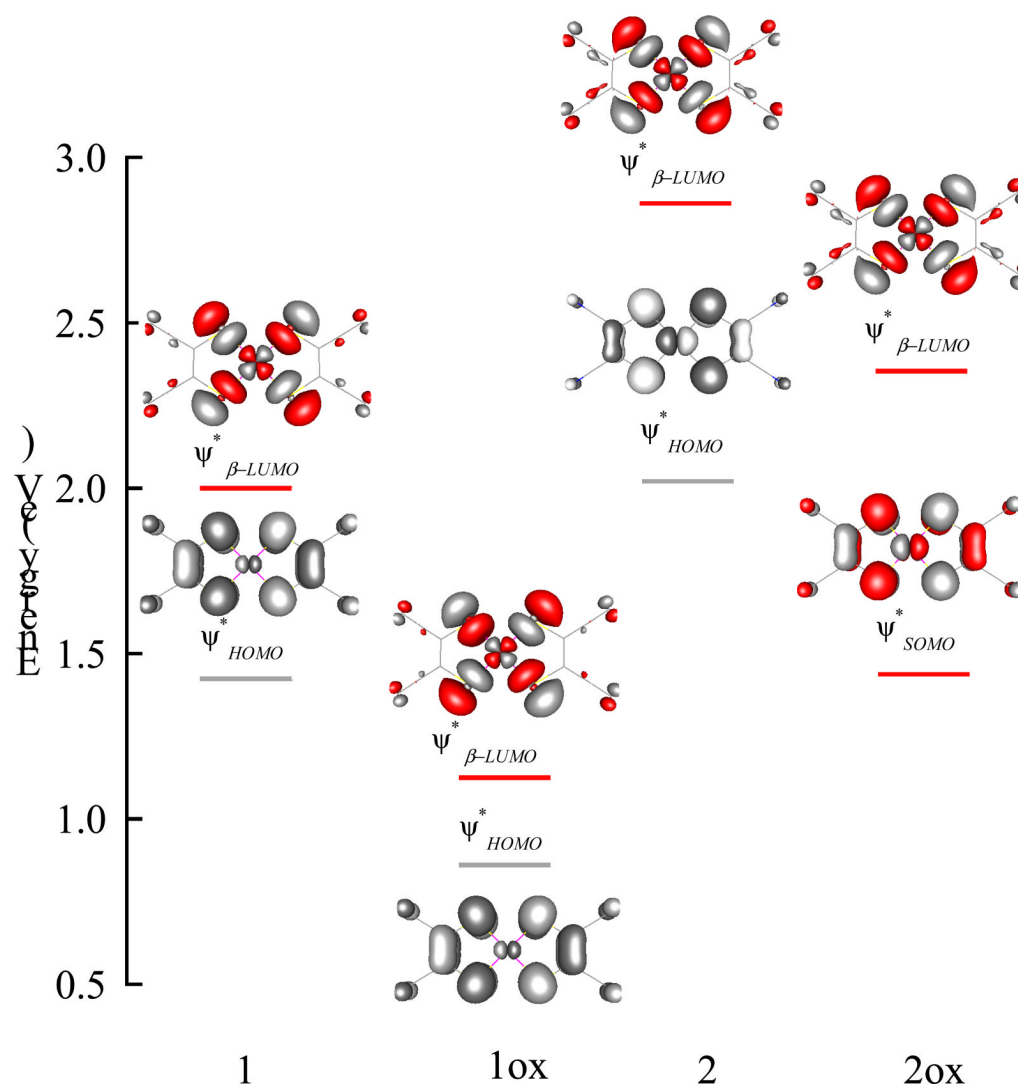
Figure 5.
Orbital contour plots of the spin-unrestricted broken symmetry wave functions for **1-2ox**. The relative energy positions of the orbitals have been obtained by aligning the N 1s energy in each case. Singly and doubly unoccupied orbitals which have been probed by S K-edge XAS are shown in red.
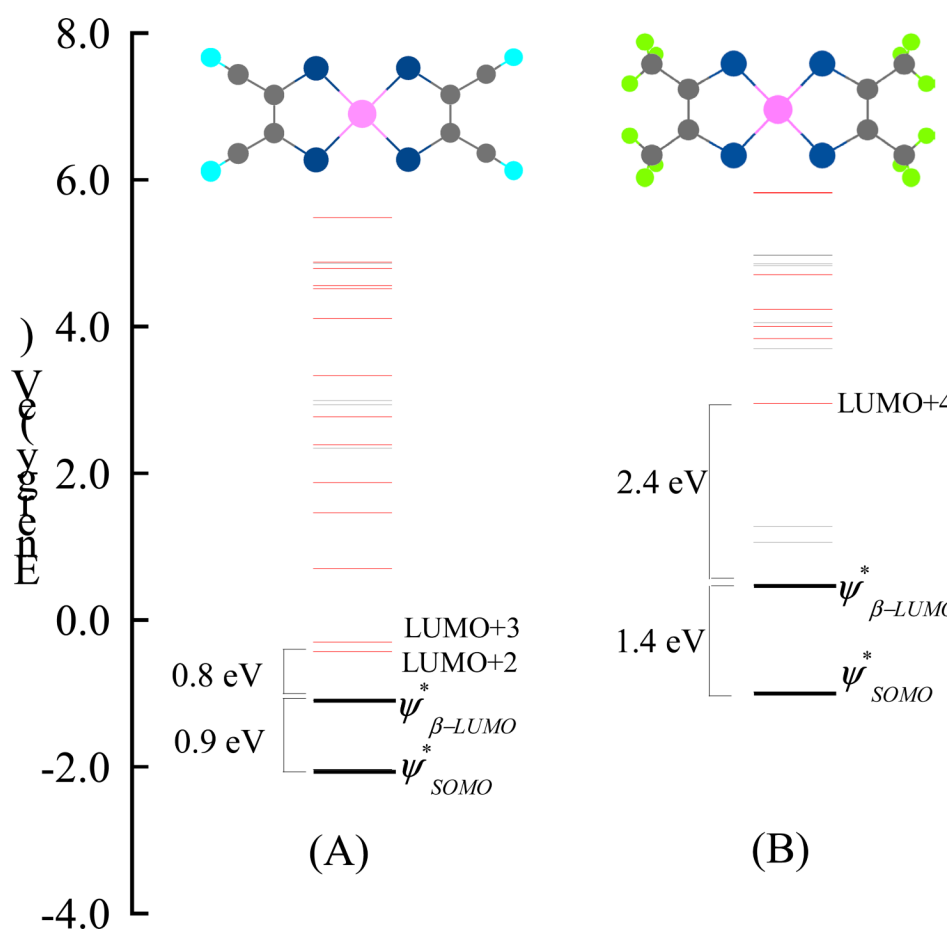
Figure 6.
DFT calculated energy level diagram of **2ox** (**A**) and (NEt$_4$)[Ni(S$_2$C$_2$Me$_2$)$_2$] (**B**). The orbitals with significant S 3p character are shown in red while those without are shown in gray. **2ox** and (NEt$_4$)[Ni(S$_2$C$_2$Me$_2$)$_2$] have been optimized under D_{2h} and C_{2v} symmetries, respectively.
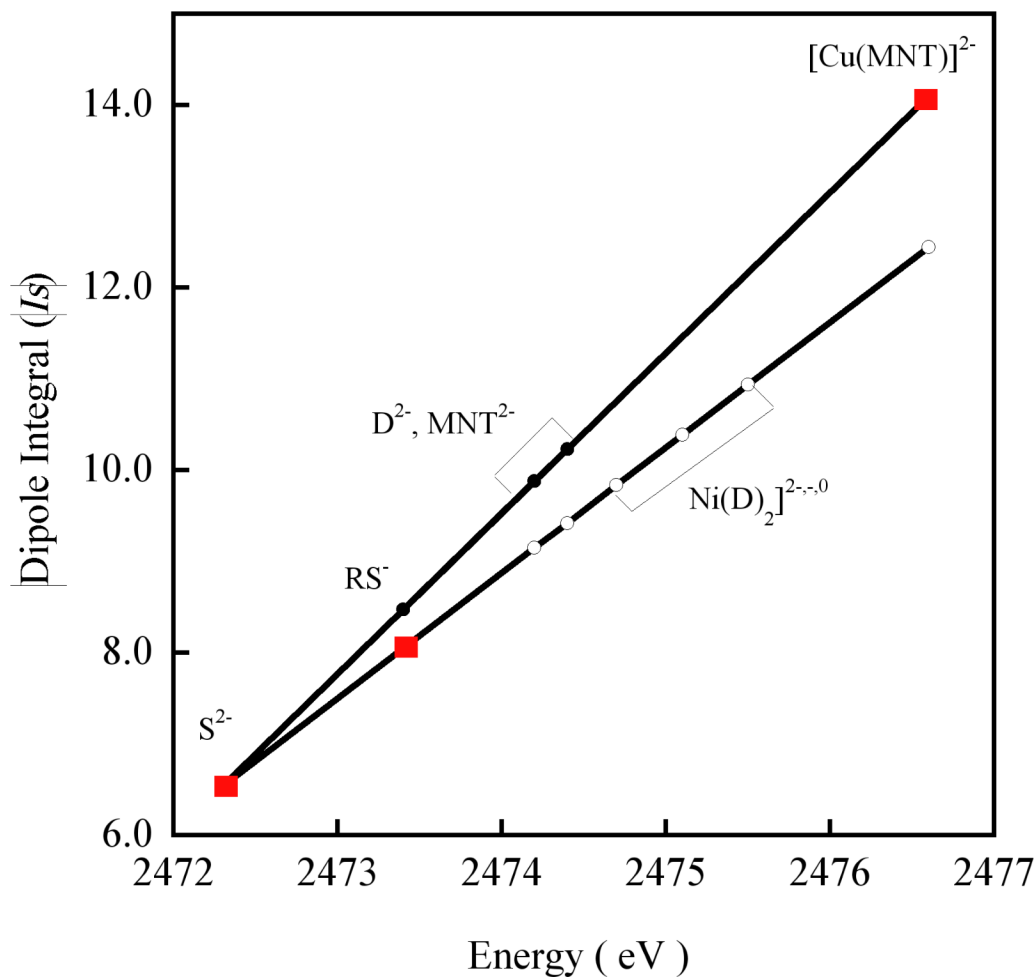
Figure 7.
Change in dipole integral (I_s) with the S 1s→4p transition energy position. The correlation developed from the I_s values for S^{2-} and RS^- (red squares) is extrapolated to compounds which have higher positive charge on S (white circles) and compared to the correlation determined from the spectroscopically derived I_s values for S^{2-} and $[Cu(MNT)]^{2-}$ (red squares). The I_s values for RS^-, D^{2-} (D is $(S_2C_2(Me)_2^{2-})$) and MNT^{2-} obtained from interpolation of the two spectroscopically determined I_s values are represented by black circles.

Table 1

Cu K- and L-edge X-ray Absorption Edge Energy Positions (eV) and Cu Character in the $\psi^{*}_{\beta-LUMO}$.

	Cu K-edge[a]			Cu L-edge[b]		
	1s→4p	2p→3d		Cu Character in $\psi^{*}_{\beta-LUMO}$ (per − hole)[c]		
Complex	1s→3d	+ shakedown	L₃ edge	L₂ edge		
1	8979.3	8985.0	931.7	951.7	39%	
1ox	8980.7	8986.6	933.3	953.3	28%	

[a] Energy resolution ~1 eV.

[b] Energy resolution ~0.1 eV.

[c] Error in total intensity due to data processing and fitting is ±3%.

Table 2

S K-X-ray Absorption Edge Energy Positions and Pre-edge Intensities

Complex	S-K Pre-edge[a] Energy (eV)	Rising-edge Energy (eV)[b]	Total Pre-edge Intensities[c]
$(TBA)_2[Cu(MNT)_2]$	2470.4	2471.5	0.63
$(TBA)[Cu(MNT)_2]$	2470.1	2472.1	1.41
$(NEt_4)_2[Ni(MNT)_2]$	2471.2	2471.8	0.99
$(NEt_4)[Ni(MNT)_2]$	2470.2[d]	2472.1	0.83[d]
	2471.0[e]		1.10[e]

[a]Energy resolution ~0.2 eV.

[b]Lowest energy edge transition.

[c]Error in total intensity due to data processing and fitting is ± 3%.

[d]The lower and higher energy pre-edge peaks, respectively.

[e]The lower and higher energy pre-edge peaks, respectively.

Table 3

Selected DFT Parameters.

Complex	Cu/Ni-S Bond Distance (Å)	$\psi^*_{\beta-LUMO}$ Composition (%)[a]		
		Cu/Ni	S	L[b]
1	2.32	37.6	52.0	10.4
1ox	2.22	24.7	64.8	10.5
2	2.19	42.9	43.8	13.3
		39.5	46.2	14.3
2ox	2.17			
		31.2[c]	50.5[c]	18.2[c]

[a]Results from Mulliken population analysis.

[b]L represents the C and N atoms of the MNT ligand.

[c]ψ^*_{SOMO} compositions.

Table 4

S Character[a] in $\psi^*_{\beta-LUMO}$ Obtained from S K-edge XAS

1	1ox	2	2ox
54.0%	60.1%	42.3%	46.7% (70.7%)[b]

[a]Error in S character is ± 3%.

[b]ψ^*_{SOMO} composition is given in parenthesis